Petroleum Science 21 (2024) 2745–2757

Contents lists available at ScienceDirect

Petroleum Science

journal homepage: www.keaipublishing.com/en/journals/petroleum-science

Original Paper

Reshaping force for deformed casing repairing with hydraulic rolling reshaper and its influencing factors

Hong-Fei Li, Min Luo *, Ting-Ting Xu, Qiao-Zhen Li, Cong-Jian Huang

School of Mechanical Science and Engineering, Northeast Petroleum University, Daqing, 163318, Heilongjiang, China

ARTICLE INFO

Article history:
Received 4 September 2023
Received in revised form
4 January 2024
Accepted 23 February 2024
Available online 26 February 2024

Edited by Jie Hao and Meng-Jiao Zhou

Keywords:
Hydraulic rolling reshaper
Reshaping force
Deformed casing
Casing reshaping
Hertz contact theory

ABSTRACT

Hydraulic rolling reshaper is an advanced reshaping tool to solve the problem of casing deformation, which has been widely used in recent years. When it is used for well repair operation, the reshaping force provided by ground devices is generally determined by experience. However, too large reshaping force may destroy the deformed casing, and too small reshaping force may also prolong the construction period and affect the repairing effect. In this paper, based on Hertz contact theory and elastic-plastic theory, combined with the process parameters of shaping, and considering the structural characteristics of the deformed casing and reshaper, we propose a mathematical model for calculating the reshaping force required for repairing deformed casing by hydraulic rolling reshaper. Meanwhile, the finite element model and numerical method of hydraulic rolling reshaper repairing deformed casing are established by using the finite element method, and the reliability of the mathematical model is verified by several examples. On this basis, the control variable method is used to investigate the influence of each parameter on the reshaping force, and the influence degree of each parameter is explored by orthogonal simulation test and Pearson correlation analysis. The research results not only provide an important theoretical basis for the prediction of reshaping force in on-site construction, but also provide a reference for the subsequent improvement of the shaping process.

1. Introduction

In recent years, with the continuous development of oilfields, the gradual deterioration of the downhole working environment has led to a continuous increase in the number of casing damages. According to the statistical data of oilfields over the years at home and abroad, the number of wells with deformed casing accounts for more than half of the number of wells with damaged casing (Peng et al., 2007; Xu et al., 2009; Tao, 2015; Wang et al., 2022). If the deformed casing is not effectively repaired in time, the casing failure is easy to occur, so the repair of deformed casing has become an important problem to be solved urgently in oilfield development (Deng et al., 2018; Zhou et al., 2019).

After years of exploration and practice, researchers have developed various reshaping tools such as pear-shaped expander, off-center tube expander, rotary cam casing swage, split tube expander and so on (Jiang, 2003; Denney, 2012; Han et al., 2018; Yu, 2017; Lei et al., 2020; Forbes, 2021). According to their working principles, it can be seen that the reasonable reshaping force provided by ground devices is crucial in the construction process. If the reshaping force is too large, the casing deformation will be further developed into casing damage, which will make the workover process more complicated and difficult (Wu and Liu, 2005). If the reshaping force is too small, the repairing process requires multiple trips to the well, which will prolong the construction period of the workover and reduce the repairing efficiency. For this reason, many studies have focused on how to determine the reshaping force required to repair the deformed casing. Pear-shaped expander is the earliest proposed and put into use, which has been widely used due to its simple structure, durability and low price, and the research on its reshaping force is also in-depth. Some scholars (Lin et al., 2013; Deng et al., 2016, 2019) have adopted theoretical analysis and numerical simulation methods to obtain the required expansive force of the pear-shaped expander, and verified the correctness of the calculation method by finite element analysis. For other traditional reshaping tools, such as off-center tube expander and split tube expander, the reshaping force required to repair the deformed casing has also been obtained by force analysis of the expanding head or part of the splitting head (Zhang, 2011).

* Corresponding author.
E-mail address: luomin@nepu.edu.cn (M. Luo).

https://doi.org/10.1016/j.petsci.2024.02.011

Some useful research results have been obtained through previous studies, but for the traditional reshaping tools mentioned above, it is found that there are common problems such as high construction risk, long construction period and high cost in the process of practical application (Yu et al., 2011). Therefore, with the development of reshaping tools and the progress of workover technique, hydraulic rolling reshaper have emerged as the times require, and due to its construction safety, short shaping period and low construction cost, it has become an important reshaping tool to solve the problem of casing deformation, especially for repairing horizontal wells (Liu et al., 2011). However, according to the published reports, most studies on reshaping force have focused on traditional reshaping tools. In addition, the research on hydraulic rolling reshaper is limited to the simulation analysis of the shaping process (Luo et al., 2016; Jin, 2022), the research on its reshaping force by theoretical analysis is rarely reported, and the reshaping force is often determined by experience during on-site construction. Hence, to better guide on-site construction, it is clear that we are in need to carry out the mechanical analysis on the process of repairing deformed casing by hydraulic rolling reshaper, focusing on solving the problem that the reshaping force often depends on experience.

In this paper, based on Hertz contact theory and elastic-plastic theory, a new mathematical model is established to calculate the reshaping force required for repairing deformed casing by hydraulic rolling reshaper, which aims to provide a theoretical basis for the prediction of the reshaping force. To verify the reliability of the mathematical model, the finite element model and numerical method for repairing deformed casing by hydraulic rolling reshaper are established to calculate and compare the simulated and theoretical results under different working conditions. According to the mathematical model established in this study, the control variable method is used to explore the relationships between multiple parameters and reshaping force, and the influence degree of each parameter on the reshaping force is quantitatively judged by orthogonal simulation test and Pearson correlation analysis.

2. Mathematical model of reshaping force

The basic components of hydraulic rolling reshaper include an anchoring device, a hydraulic booster cylinder and a reshaping head, and the anchoring device is threaded to the drill pipe, as shown in Fig. 1. When the hydraulic rolling reshaper is lowered into the deformed section of the casing, the anchoring device anchors the reshaper and pushes the expansive body in the reshaping head under the action of the hydraulic booster cylinder, so that the balls are extruded from the reshaping head. The load and torque required for shaping are provided by the minor workover rig and pump motor on the ground, then the reshaper can drill spirally at a certain speed, and the high stress generated by multi-stage ball rolling the deformed section causes plastic deformation of the casing to achieve the shaping requirements.

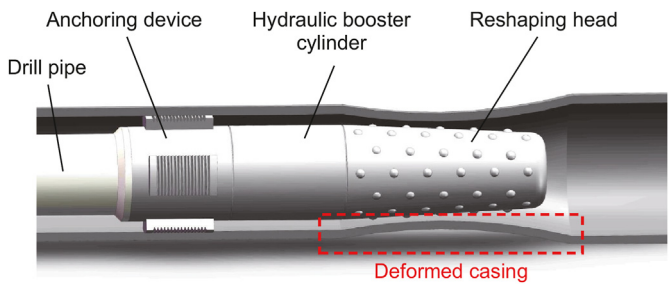

Fig. 1. Working principle of hydraulic rolling reshaper.

Based on its working principle, it can be seen that the balls embedded in the reshaping head are the key components which are in direct contact with the inner wall of the casing, and they are also the main body of transmitting the reshaping force to achieve the repairing goal. Hence, the multi-stage balls on the reshaper and deformed casing are selected as the research objects, the mechanical properties of the casing are reflected in the flow stress, and the mechanical analysis of the surface contact between the balls and the inner wall of the deformed casing is carried out based on Hertz contact theory. According to the working principle and structural characteristics of the reshaper, combined with the process parameters of shaping, the calculation method of the spatial spiral curve formed by rolling is proposed. The contact duration between the reshaper and the casing is derived based on the geometric relationship, which is taken as the integrated range of the spatial curve, and then the spiral contact area of the contact pair is solved. According to the elastic-plastic theory, the stress distribution of the casing under the internal pressure is analyzed by considering Mises yield condition and Tresca yield condition comprehensively, and then the plastic limit internal pressure required to repair the deformed casing is determined. Finally, a mathematical model is presented that could calculate the reshaping force required for repairing deformed casing by hydraulic rolling reshaper. The flow chart of modeling is shown in Fig. 2, and the details are presented below.

2.1. Surface contact analysis

In the shaping process, the balls of the ith stage first contact with the inner wall of the casing with the movement of the reshaper. To facilitate the analysis of the contact mechanics between the reshaper and the inner wall of the deformed casing, taking a single ball as an example, and the deformed section of the casing is simplified as a circular arc. The curvature radius of the deformed section in contact with the balls of the ith stage is R_i, the radius of the ball is R_b, and the initial contact state is shown in Fig. 3. The contact starts as a point contact, and the contact point is O_{12}, which is located on the common tangent plane $\Gamma_1\Gamma_2$ of the contact.

The distance between the two points M_1 and M_2 on the deformed casing and the ball from the common normal X_1X_2 are set to r, then Eq. (1) can be obtained from the geometrical relationship:

$$(R_b - Z_1)^2 + r^2 = R_b^2, (R_i - Z_2)^2 + r^2 = R_i^2 \tag{1}$$

If M_1 and M_2 are close to the contact point O_{12}, Z_1 is much less than $2R_b$, and Z_2 is much less than $2R_i$. Hence, Eq. (1) is simplified, and the distance between M_1 and M_2 is obtained as follows:

$$Z_1 + Z_2 = \left(\frac{R_b + R_i}{2R_bR_i}\right)r^2 = \beta_{12}r^2, \beta_{12} = \frac{R_b + R_i}{2R_bR_i} \tag{2}$$

When there is no pressure between the contact pairs, the balls and the deformed casing are in point contact. With the continuous feed of the reshaper, the two extrude each other, and local deformation will inevitably occur near the contact point. The initial point contact will be expanded into a surface contact with a circular boundary, and the load will be distributed from the concentrated load to the whole contact surface. Accordingly, the distance between the center O_1 of the ball and the center O_2 of the curvature radius of the deformed section is set to α_{12}, and the displacements of points M_1 and M_2 relative to their circle centers O_1 and O_2 along the common normal are set to u_{z1} and u_{z2}. With the extrusion of the ball, the distance between M_1 and M_2 is shortened to become the same point M on the contact surface, then Eq. (3) is obtained:

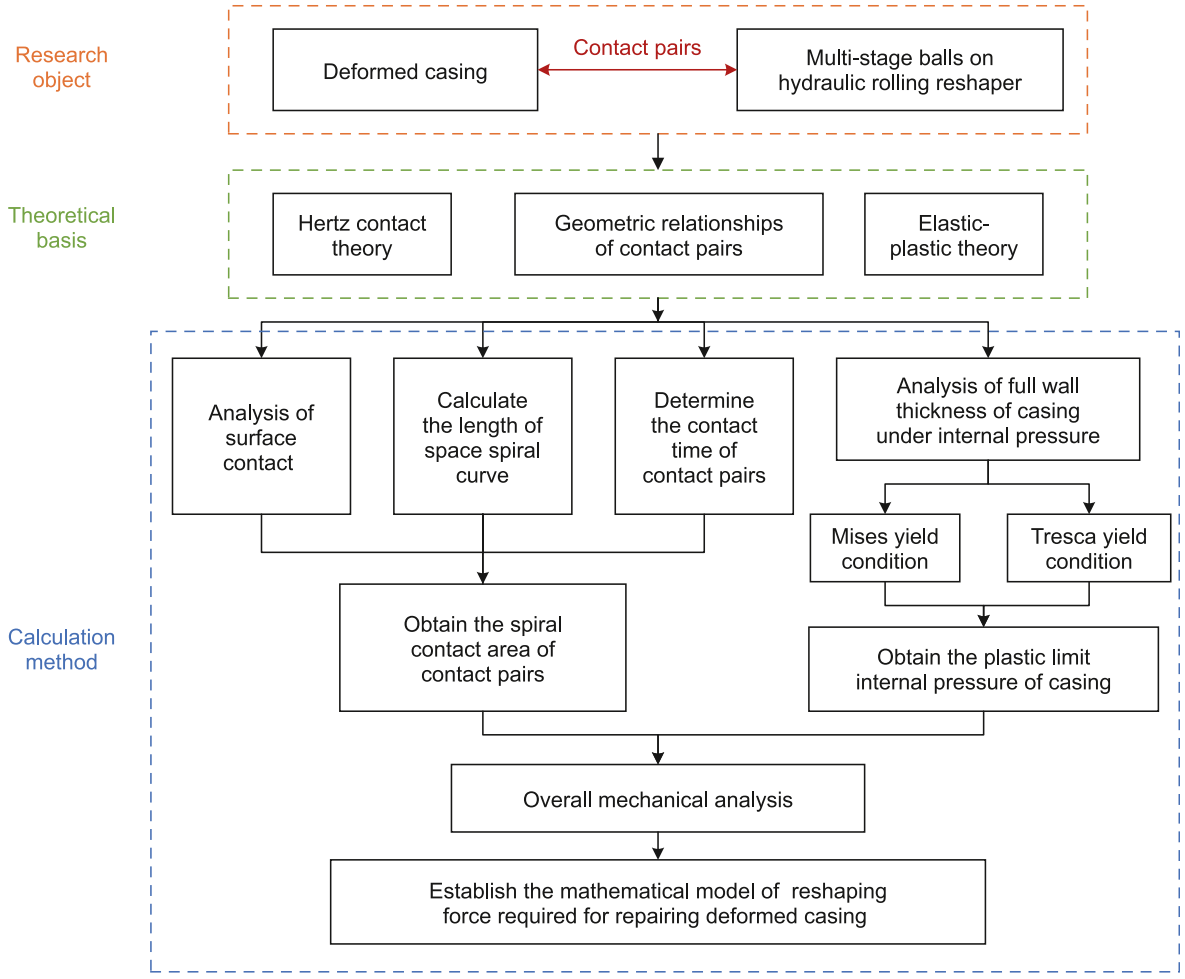

Fig. 2. Flow chart of modeling.

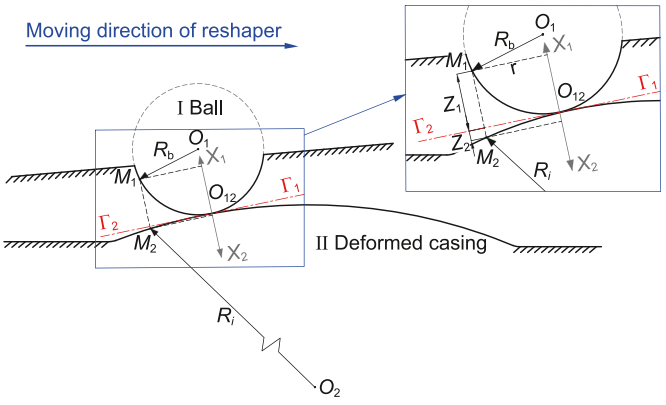

Fig. 3. Initial contact state of the ball with the inner wall of the casing.

$$u_{z1}+u_{z2}=\alpha_{12}-(Z_1+Z_2)=\alpha_{12}-\beta_{12}r^2 \tag{3}$$

The contact surface between the ball and the deformed casing is shown in Fig. 4, the radius of the contact circle is r_{12}, and the normal pressure on the contact surface is $q(r)$.

Fig. 4(a) shows a hemispherical surface on the contact surface, and the height of the hemispherical surface at each point represents the magnitude of the pressure q at that point. According to Hertz contact theory, under the action of extrusion force F_N, the normal stress distribution in the contact area is shown in Eq. (4), and the contact stress at the contact center is the largest, corresponding to the height of the hemispherical surface at the contact point O_{12}, and the maximum contact stress is shown in Eq. (5) (Harris and Kotzalas, 2007). The change of pressure is shown as the semicircle dashed line in Fig. 4(b), and the integral along the chord Q_1Q_2 is given in Eq. (6).

$$q(x,y)=\frac{3F_N}{2\pi r^2}\left[1-2\left(\frac{x}{r}\right)^2\right]^{\frac{1}{2}} \tag{4}$$

$$q_{max}=\frac{3F_N}{2\pi r_{12}^2} \tag{5}$$

$$\int q(r)\mathrm{d}s=\frac{q_{max}}{r_{12}}A=\frac{\pi q_{max}}{2r_{12}}\left(r_{12}^2-r^2\sin\psi\right) \tag{6}$$

where A is the area of the semicircle, mm^2, and the radius of the semicircle is $\sqrt{r_{12}^2-r^2\sin\psi}$ based on the geometric relationship; $q(r)$ is the contact pressure distribution on the contact surface, N.

The mechanical problem of repairing the deformed casing by the reshaper is the space axisymmetric problem. Therefore, according to the differential equation of the axisymmetric body in the elastic half-space (Xu, 2006), combined with the displacement

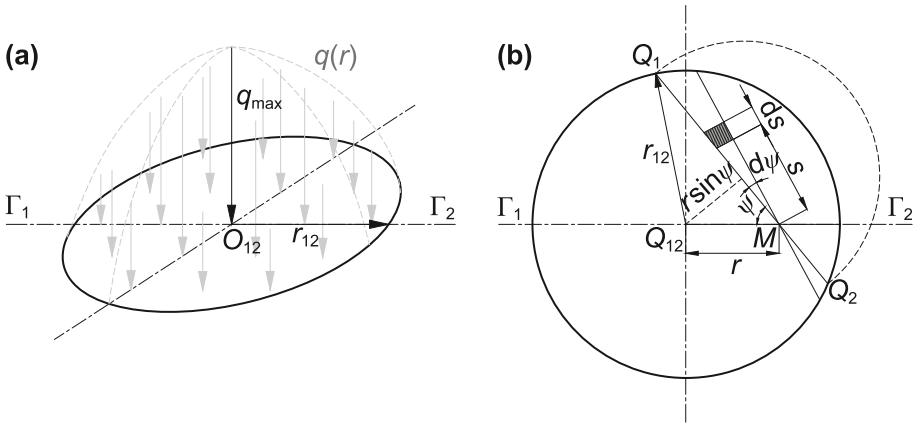

Fig. 4. Schematic diagram of contact surface $\Gamma_1\Gamma_2$. **(a)** Distribution of contact pressure. **(b)** Infinitesimal integral of circular domain.

potential function and the Love displacement function, and the Boussinesq solution for the half-space body subjected to a concentrated force is obtained by using the superposition method. According to the expression of the axial displacement component therein, the displacement distributions on the contact surface are integrated to obtain the axial displacements of M_1 and M_2 under the action of concentrated force as follows:

$$u_{z1}=\frac{1-\mu_1^2}{\pi E_1}\iint q(r)\mathrm{d}s\mathrm{d}\psi,\ u_{z2}=\frac{1-\mu_2^2}{\pi E_2}\iint q(r)\mathrm{d}s\mathrm{d}\psi \tag{7}$$

where μ_1 and μ_2 are the Poisson's ratios of the ball and deformed casing; and E_1 and E_2 are the elastic modulus of the ball and deformed casing, MPa.

From Eq. (7), Eq. (8) is obtained:

$$\begin{cases} u_{z1}+u_{z2}=(k_1+k_2)\iint q(r)\mathrm{d}s\mathrm{d}\psi \\ k_1=\dfrac{1-\mu_1^2}{\pi E_1},k_2=\dfrac{1-\mu_2^2}{\pi E_2} \end{cases} \tag{8}$$

From Eqs. (1), (6) and (8), Eq. (9) is obtained:

$$(k_1+k_2)\frac{\pi^2 q_{\max}}{4r_{12}}\left(2r_{12}^2-r^2\right)=\alpha_{12}-\beta_{12}r^2 \tag{9}$$

Let the coefficients of the constant term and the r^2 term at the left and right ends of Eq. (9) be equal, and then Eq. (10) can be obtained:

$$\alpha_{12}=(k_1+k_2)\frac{\pi^2 q_{\max} r_{12}}{2},\beta_{12}=(k_1+k_2)\frac{\pi^2 q_{\max}}{4r_{12}} \tag{10}$$

Substituting Eqs. (2) and (5) into Eq. (10), and the radius of the contact circle r_{12} is obtained:

$$r_{12}=\left[\frac{3\pi R_b R_i(k_1+k_2)F_N}{4(R_b+R_i)}\right]^{\frac{1}{3}} \tag{11}$$

Then the maximum contact stress $q_{\max}$ on the contact surface can be obtained as follows:

$$q_{\max}=\frac{3F_N}{2\pi}\left[\frac{4(R_b+R_i)}{3\pi R_b R_i(k_1+k_2)F_N}\right]^{\frac{2}{3}} \tag{12}$$

To meet the requirement of not damaging the casing and achieving the corresponding shaping effect, the maximum contact stress should meet the requirement of $\sigma_s<q_{\max}<\sigma_b$, where σ_s and σ_b are the yield strength and strength limit of the casing, respectively. Hertz contact theory is applicable to analyze elastic contact problems, but the casing needs to be plastically deformed to achieve the purpose of reshaping in the process of casing repair (Deng et al., 2019). Therefore, this study uses the flow stress σ_f to represent the stress level between σ_s and σ_b (Zhu and Leis, 2005):

$$\sigma_f=(\sigma_s+\sigma_b)/2 \tag{13}$$

Therefore, from Eqs. (11)–(13), the diameter of the contact circle between the single ball of the ith stage and the inner wall of the casing is obtained as follows:

$$d_i=\frac{\sigma_f\pi^2 R_b R_i(k_1+k_2)}{R_b+R_i} \tag{14}$$

where d_i is the diameter of the contact circle between the single ball of the ith stage and the inner wall of the casing, mm; σ_f is the flow stress, MPa; R_b is the radius of the ball, mm; and R_i is the curvature radius of the deformed section when the deformed casing is in contact with the balls of the ith stage, mm, calculated by the formula in Eq. (18).

2.2. Calculation of spiral contact area

From the working principle of the reshaper, it can be seen that the reshaper is extruded to form multiple spiral pits on the inner wall of the casing during the shaping process, and the reshaper with the taper of α is simplified to the frustum of a cone shown in Fig. 5(a). The diameter of the top surface of the frustum of a cone is equal to the equivalent diameter of the ith stage D_i, and the space rectangular coordinate system is established at the bottom center of the cone, where the x and y axes are located in the bottom and orthogonal to each other, and the z-axis points upward along the axis of the frustum of a cone.

The motion time of the reshaper is set to t, the axial translational velocity of the reshaper is set to v, and the rotating angular velocity is set to ω. In the beginning, the moving point is located at point K. After the moment of t, the moving point moves along the $-z$ direction and rotates around the z-axis to point K', and the vertical plane formed by point K' and the z-axis is shown in Fig. 5(b). According to the geometric relationship, the parametric equation of the spiral curve is determined as follows:

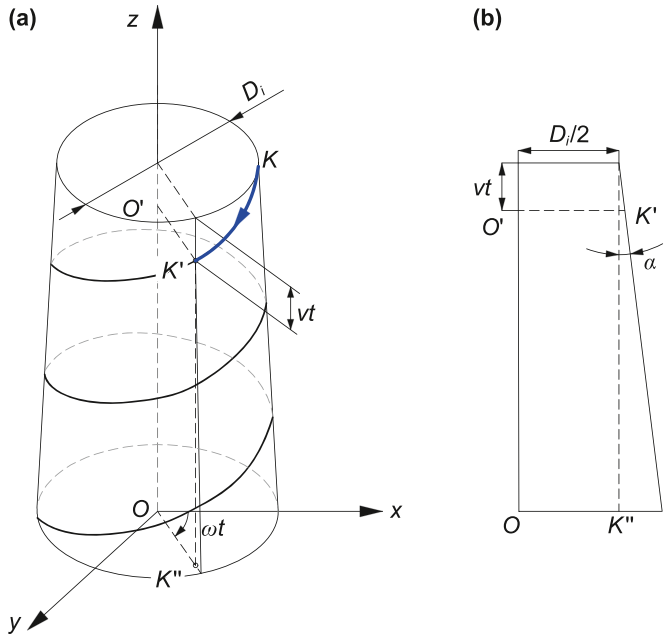

Fig. 5. Schematic diagram of the spatial spiral curve. **(a)** Spiral curve. **(b)** Vertical plane where K' is located.

$$\begin{cases} x = \left(\dfrac{D_i}{2} + vt\tan\alpha\right)\cos\omega t \\ y = \left(\dfrac{D_i}{2} + vt\tan\alpha\right)\sin\omega t \\ z = vt \end{cases} \tag{15}$$

Taking t as the integration variable, the differential of the spatial spiral curve is obtained as follows:

$$\mathrm{d}l = \sqrt{x'(t)^2 + y'(t)^2 + z'(t)^2}\,\mathrm{d}t \tag{16}$$

The contact duration between the balls of the ith stage and the inner wall of the casing is set to t_i, and the spatial spiral curve l_i of the contact between the balls of the ith stage and the inner wall of the casing is obtained as follows:

$$l_i = \frac{1}{2}\int_0^{t_i} \sqrt{4v^2(\tan^2\alpha + 1) + \omega^2(D_i + 2vt\tan\alpha)^2}\,\mathrm{d}t \tag{17}$$

The contact duration t_i is calculated below. Before reshaping, the axial deformation length of the deformed casing is L_A, the minimum diameter of the deformed casing is d_m, and the inner diameter of the intact casing is d_{in}. The minimum diameter of the casing will be changed after the balls of each stage rolling, then the minimum diameter of the casing is set to d_{mi} when the ith stage is reshaped, as shown in Fig. 6.

Based on the geometric relationship, the curvature radius of the deformed section R_i is obtained as shown in Eq. (18):

$$R_i = \frac{L_A^2 + (d_{in} - d_{mi})^2}{4(d_{in} - d_{mi})} \tag{18}$$

At the beginning of the shaping process, the cross-section where the first stage of the reshaper is located coincides with the cross-section of the connection between the deformed section and the intact section of the casing, and the plane rectangular coordinate

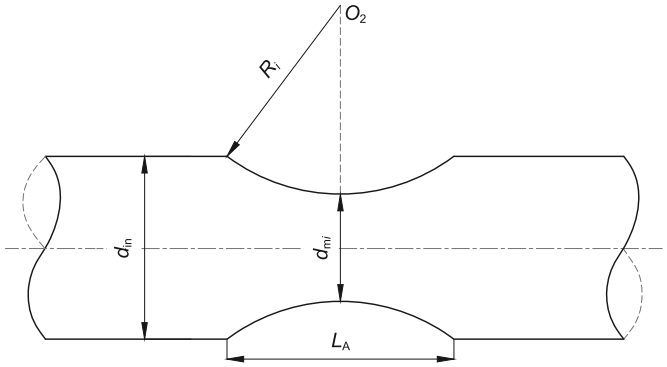

Fig. 6. Schematic diagram of the deformed section of the casing.

system is established based on this initial position and the axis of the casing. When the forward distance of the reshaper is x_1, the balls of the ith stage begin to contact with the inner wall of the casing, and the contact point is P_1 (a, b), as shown in Fig. 7.

The reshaper has a total of n-stage balls, the total length of the reshaper is L (the axial distance from the first to the last stage is the total length of the reshaper), the axial distance between the first stage and the ith stage is L_i, and the axial distance between each stage on the reshaper is uniformly distributed, and then the relationship of Eq. (19) is obtained:

$$L_i = \frac{(i-1)L}{n-1} \tag{19}$$

The equivalent diameter of the first stage is D_1, and then the equivalent diameter of the ith stage D_i can be obtained:

$$D_i = D_1 + 2L_i\tan\alpha \tag{20}$$

According to the triangle similarity principle ($\Delta O_b B P_1$ and $\Delta O_2 A P_1$), the following relation can be obtained:

$$\frac{b - D_i/2 + R_b}{R_i + d_{mi}/2 - b} = \frac{a + L_i - x_1}{L_A/2 - a} = \frac{R_b}{R_i} \tag{21}$$

The deformed section of the casing is a part of the circle, and the center of the circle is O_2 (O_x, O_y). Therefore, from the geometric relationship, $O_x = L_A/2$, $O_y = R_i + d_{mi}/2$, and P_1 is located on the circle, then Eq. (22) is obtained:

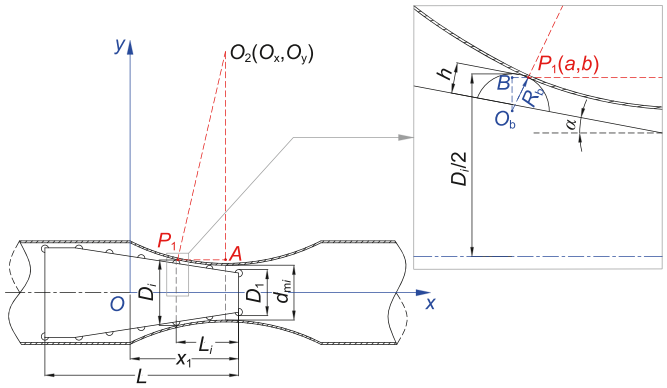

Fig. 7. State of initial contact between the balls of the ith stage and the inner wall of the casing.

$$\left(a-\frac{L_A}{2}\right)^2+\left[b-\left(R_i+\frac{d_{mi}}{2}\right)\right]^2=R_i^2 \tag{22}$$

From Eqs. (21) and (22), the coordinates of P_1 are obtained:

$$a=\frac{R_i(d_{mi}-D_i)}{2(R_i+R_b)}\sqrt{\frac{4(R_i+R_b)}{D_i-d_{mi}}-1}+\frac{L_A}{2},\ b=\frac{R_b d_{mi}+R_i D_i}{2(R_i+R_b)} \tag{23}$$

Hence, from Eq. (21), x_1 is obtained as follows:

$$x_1=(d_{mi}-D_i)\sqrt{\frac{R_i+R_b}{D_i-d_{mi}}-1}+\frac{1}{2}L_A+L_i \tag{24}$$

When the balls of the ith stage are about to separate from the inner wall of the casing, the forward distance of the reshaper is set to x_2. From Eq. (24), x_2 is obtained:

$$x_2=(D_i-d_{mi})\sqrt{\frac{R_i+R_b}{D_i-d_{mi}}-1}+\frac{1}{2}L_A+L_i \tag{25}$$

The contact length of reshaping is the difference between x_2 and x_1. Therefore, from Eqs. (24) and (25), the contact duration t_i is obtained:

$$t_i=\frac{2(D_i-d_{mi})}{v}\sqrt{\frac{R_i+R_b}{D_i-d_{mi}}-1} \tag{26}$$

From Eqs. (14), (17), (19), (20) and (26), the contact area S_i between the balls of the ith stage and the inner wall of the casing is obtained:

$$S_i=\frac{\sigma_f\pi^2R_bR_i(k_1+k_2)m}{2(R_b+R_i)}\int_0^{t_i}\sqrt{4v^2(\tan^2\alpha+1)+\omega^2(D_i+2vt\tan\alpha)^2}\mathrm{d}t \tag{27}$$

where m is the number of balls per stage, and the number of balls in each stage on the hydraulic rolling reshaper is the same.

2.3. Plastic limit internal pressure analysis of full-wall casing

In the process of casing shaping, the casing will undergo the process from inner-wall yield to full-wall yield. Hence, the elastic-plastic mechanical response of the casing subjected to internal pressure is investigated below, and the plastic limit internal pressure of the casing under two yield conditions is calculated.

The inner radius of the minimum diameter of the casing is ρ_{i1}, the outer radius is ρ_{i2}, and the inner wall is subjected to the repair pressure p. According to the force condition and geometric shape of the casing, ignoring the complex stress distribution near both ends of the casing due to constraints, it can be seen that the casing is in an axisymmetric plane strain state. Therefore, the cylindrical coordinate system (ρ,θ,z) is used for analysis, so that the z-axis coincides with the axis of the casing, and the polar coordinate system is in the cross-section of the casing, with the radial coordinate of the cross-section as ρ, and the circumferential coordinate as θ. Without considering physical force, the equilibrium equation is obtained:

$$\frac{\mathrm{d}\sigma_\rho}{\mathrm{d}\rho}+\frac{\sigma_\rho-\sigma_\theta}{\rho}=0 \tag{28}$$

From the stress component formulas of cartesian coordinates, the stress components expressed by the stress functions in polar coordinates are obtained by coordinate transformation. For the axisymmetric problem of repairing the deformed casing, the stress distribution is independent of θ, and the stress function is only a function of ρ, so there are only radial stress and circumferential stress in the cross-section of the casing, as shown in Eq. (29).

$$\sigma_\rho=\frac{1}{\rho}\frac{\partial\varphi}{\partial\rho},\ \sigma_\theta=\frac{\partial^2\varphi}{\partial\rho^2} \tag{29}$$

According to the deformation compatibility equation, the stress function is expressed as follows (Li, 2014):

$$\varphi=A\ln\rho+B\rho^2\ln\rho+C\rho^2+D \tag{30}$$

Since the casing is a continuum, the single-valued condition of displacement is satisfied, and the term of $B\rho^2\ln\rho$ in the stress function is 0. Due to the boundary conditions (Eq. (31)), Eq. (32) can be obtained:

$$\sigma_\rho|_{\rho=\rho_{i1}}=-p,\tau_{\rho\theta}|_{\rho=\rho_{i1}}=\tau_{\rho\theta}|_{\rho=\rho_{i2}}=0 \tag{31}$$

$$A=\frac{\rho_{i1}^2\rho_{i2}^2p}{\rho_{i1}^2-\rho_{i2}^2},C=\frac{\rho_{i1}^2p}{2\left(\rho_{i2}^2-\rho_{i1}^2\right)} \tag{32}$$

Based on the constitutive equations of the total strain theory (Wang et al., 2006), the stress components when the casing is subjected to internal pressure are obtained:

$$\begin{cases}\sigma_\rho=\dfrac{p\rho_{i1}^2}{\rho_{i2}^2-\rho_{i1}^2}\left(1-\dfrac{\rho_{i2}^2}{\rho^2}\right)\\ \sigma_\theta=\dfrac{p\rho_{i1}^2}{\rho_{i2}^2-\rho_{i1}^2}\left(1+\dfrac{\rho_{i2}^2}{\rho^2}\right)\\ \sigma_z=\dfrac{1}{2}(\sigma_\rho+\sigma_\theta)=\dfrac{p\rho_{i1}^2}{\rho_{i2}^2-\rho_{i1}^2}\end{cases} \tag{33}$$

From Mises yield condition, Eq. (34) is obtained:

$$\overline{\sigma}=\sqrt{\frac{1}{2}\left[(\sigma_\theta-\sigma_\rho)^2+(\sigma_\theta-\sigma_z)^2+(\sigma_\rho-\sigma_z)^2\right]}=\frac{\sqrt{3}\rho_{i1}^2\rho_{i2}^2}{\rho_{i2}^2-\rho_{i1}^2}\frac{p}{\rho^2} \tag{34}$$

Under the action of internal pressure p, a plastic zone is formed in the inner wall of the casing when the maximum stress generated in the inner wall exceeds the yield strength. With the increase of internal pressure, the plastic zone expands outward, creating the coexistence of elastic and plastic zones in the casing as shown in Fig. 8.

In the plastic zone, the casing is in the yield state, and Eq. (35) is obtained from Eqs. (33) and (34):

$$\sigma_\theta-\sigma_\rho=\frac{2}{\sqrt{3}}\sigma_s \tag{35}$$

From the boundary condition of Eq. (31), substituting Eq. (35) into Eq. (28) and integrating to obtain Eq. (36) as follows:

$$\sigma_\rho=\frac{2}{\sqrt{3}}\sigma_s\ln\frac{\rho}{\rho_{i1}}-p \tag{36}$$

With the increase of internal pressure, the plastic zone of the casing extends outward and finally extends to the outer wall ($\rho=\rho_{i2}$), at which time the casing reaches the plastic limit. However, the stress of the casing needs to reach the tensile limit in the process of shaping (Lin, 2016). Therefore, in the limit state, the plastic limit

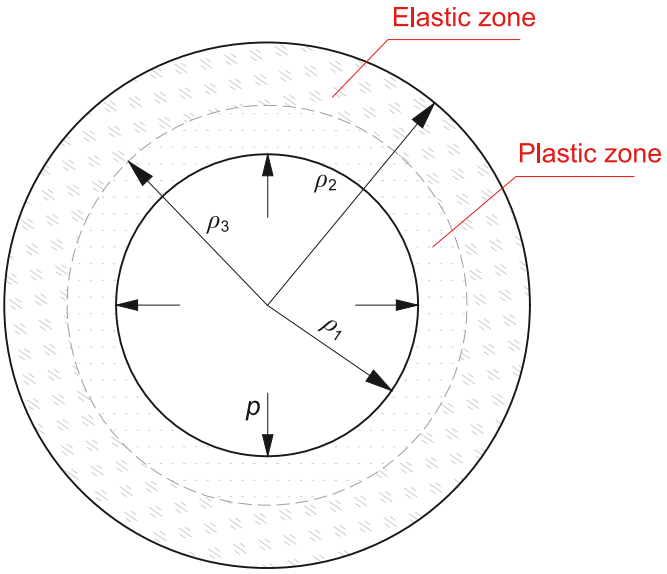

Fig. 8. Elastic-plastic zone of the casing under internal pressure.

internal pressure required for the balls of the *i*th stage to repair the deformed casing under Mises yield condition is obtained:

$$p_{bi}^1 = \frac{2}{\sqrt{3}}\sigma_b \ln\frac{\rho_{i2}}{\rho_{i1}} \tag{37}$$

If Tresca yield condition is applied, Eq. (38) is obtained:

$$\sigma_\theta - \sigma_\rho = \sigma_s \tag{38}$$

The equilibrium equation of Eq. (28) is still tenable for the plastic zone, and from Eq. (31), Eq. (39) is obtained after integration:

$$\sigma_\rho = \sigma_s \ln\frac{\rho}{\rho_{i1}} - p \tag{39}$$

Similarly, with the increase of internal pressure, the plastic limit internal pressure under Tresca yield condition is obtained as follows:

$$p_{bi}^2 = \sigma_b \ln\frac{\rho_{i2}}{\rho_{i1}} \tag{40}$$

By comparing Eqs. (37) and (40), it is found that the plastic limit internal pressure obtained by Mises yield condition is larger than that obtained by Tresca yield condition, so the result calculated by Eq. (37) is more radical than Eq. (40). By comprehensively considering the calculation methods proposed under two yield conditions, and through the calculation and comparison of Section 3.2. In this paper, it is considered that it is more reliable to calculate the plastic limit internal pressure required for repairing casing by considering the average results of both methods. Therefore, the plastic limit internal pressure required for the balls of the *i*th stage to repair the deformed casing is determined as shown in Eq. (41).

$$p_{bi} = \frac{1}{2}\left(p_{bi}^1 + p_{bi}^2\right) = \left(\frac{\sqrt{3}}{3} + \frac{1}{2}\right)\sigma_b \ln\frac{\rho_{i2}}{\rho_{i1}} \tag{41}$$

2.4. Calculation of reshaping force

Fig. 9 shows the overall mechanical model of repairing deformed casing by hydraulic rolling reshaper. In the actual construction process, the reshaping force and torque are applied to the reshaper, and the circumferential friction force and normal extrusion force act on the inner wall of the casing under the action of reshaping force and torque, wherein the torque is used to offset the circumferential friction force, and the reshaping force acts on the deformed casing by generating extrusion force in contact with the inner wall of the casing.

Based on the mechanical analysis, the mechanical equilibrium equation is obtained as follows:

$$F = \sum_{i=1}^{k} F_i = \sum_{i=1}^{k}(F_{Ni}\sin\alpha + f_i\cos\alpha) \tag{42}$$

where F is the reshaping force required to repair the deformed casing, N; k is the maximum of stages in which the balls are in contact with the inner wall of the casing during the shaping process; F_{Ni} is the normal force required to repair the deformed casing by the balls of the *i*th stage in contact with the inner wall of the casing, N, and $F_{Ni} = p_{bi}S_i$; f_i is the sliding friction force between the balls of the *i*th stage and the inner wall of the casing, N, which can be calculated according to Coulomb law of friction $f_i = \mu F_{Ni}$, where μ is the friction coefficient; and α is the taper of the reshaper, °, for the reinforced stage of the reshaper, $\alpha = 0°$.

Therefore, from Eqs. (27), (41) and (42), the final mechanical model for calculating the reshaping force required for repairing deformed casing by hydraulic rolling reshaper is given as

$$\begin{cases} F = \sum_{i=1}^{k}(p_{bi}S_i\sin\alpha + \mu p_{bi}S_i\cos\alpha) \\ S_i = \dfrac{\sigma_f\pi^2 R_b R_i(k_1+k_2)m}{2(R_b+R_i)}\int_0^{t_i}\sqrt{4v^2\left(\tan^2\alpha+1\right)+\omega^2(D_i+2vt\tan\alpha)^2}\,dt \\ p_{bi} = \left(\dfrac{\sqrt{3}}{3}+\dfrac{1}{2}\right)\sigma_b\ln\dfrac{\rho_{i2}}{\rho_{i1}}, t_i = \dfrac{2(D_i-d_{mi})}{v}\sqrt{\dfrac{R_i+R_b}{D_i-d_{mi}}-1}, \sigma_f = (\sigma_s+\sigma_b)/2 \\ D_i = D_1 + 2\dfrac{(i-1)L}{n-1}\tan\alpha, R_i = \dfrac{L_A^2+(d_{in}-d_{mi})^2}{4(d_{in}-d_{mi})}, k_1 = \dfrac{1-\mu_1^2}{\pi E_1}, k_2 = \dfrac{1-\mu_2^2}{\pi E_2} \end{cases} \tag{43}$$

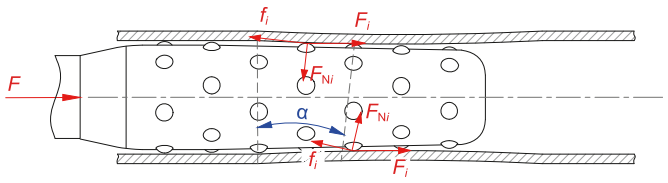

Fig. 9. Mechanical model of repairing deformed casing by hydraulic rolling reshaper.

where F is the reshaping force required to repair the deformed casing, N; n is the total number of stages of the reshaper; k is the maximum of stages in which the balls are in contact with the inner wall of the casing during the shaping process, $i = 1, 2, \ldots, k$; p_{bi} is the plastic limit internal pressure required for the balls of the ith stage to repair the deformed casing, MPa; S_i is the contact area between the balls of the ith stage and the inner wall of the casing, mm^2; μ is the friction coefficient; t_i is the contact duration, s; m is the number of balls per stage; α is the taper of the reshaper, °; v is the axial translational velocity of the reshaper, mm/s; ω is the rotating angular velocity of the reshaper, rad/s; σ_s and σ_b are the yield strength and strength limit of the casing, respectively, MPa; σ_f is the flow stress, MPa; R_i is the curvature radius of the deformed section when the deformed casing is in contact with the balls of the ith stage, mm; D_1 and D_i are the equivalent diameters of the first and ith stages, mm; d_{mi} is the minimum diameter of the casing when the balls of the ith stage repair is performed, mm; ρ_{i1} and ρ_{i2} are the inner and outer radius of the minimum diameter of the casing at the shaping process of the balls of the ith stage, mm; R_b is the radius of the ball, mm; L is the total length of the reshaper, mm; L_A is the axial deformation length of the deformed casing, mm; d_{in} is the inner diameter of the intact casing, mm; μ_1 and μ_2 are the Poisson's ratios of the ball and deformed casing; and E_1 and E_2 are the elasticity modulus of the ball and deformed casing, MPa.

3. Comparison of calculated results with simulation data

Taking a certain type of hydraulic rolling reshaper as an example, the mathematical model established in this paper is used to calculate the reshaping force required for repairing deformed casing with different degree of deformation, and the corresponding finite element model is established for simulation, and the simulated and theoretical results under different working conditions are compared and analyzed.

3.1. Example verification

3.1.1. Calculating parameters

The structural parameters of hydraulic rolling reshaper are shown in Fig. 10. The total length of the reshaper is 300 mm, the radius of the ball is 10.32 mm, and the exposed size of the ball is 5 mm. The reshaper has 7 stages, with 6 balls distributed in each stage, and the equivalent diameter of the first stage is 110 mm. Moreover, the diameters of the first 6 stages increase in steps with the taper of 1.145°, and the 7th stage is called “reinforced stage”, which is mainly used to strengthen the shaping effect of the casing, and its equivalent diameter is the same as that of the 6th stage (120 mm). Furthermore, the axial translational velocity of the reshaper is 1 mm/s, the rotating angular velocity is 0.48 rad/s, and the friction coefficient is 0.1.

According to the API 5CT standard for the material properties of the casing, the P110 casing with elastic modulus of 210 GPa, Poisson's ratio of 0.3, yield strength of 851 MPa and strength limit of 933 MPa is selected as an example for calculation. The specification of the intact casing is Φ139.7 mm × 9.17 mm, and the minimum diameter of the deformed section is located in the middle of the casing. To avoid the influence of the boundary effect, the intact casings with the length of 100 mm are connected at both ends of the deformed section, as shown in Fig. 11.

3.1.2. Theoretical calculation

Taking the deformed casing with L_A = 300 mm and d_m = 114 mm as an example, the mathematical model established in this paper is used to calculate the reshaping force.

According to the structural parameters of the reshaper, it can be seen that the 4th stage of the reshaper first contacts with the inner wall of the casing, and there are 4 stages (4th to 7th stages) of contact between the balls and the casing during the shaping process. Therefore, based on past experience, the average value of the springback of this material after shaping by single-stage balls is 0.5 mm, then according to Eq. (43) and the basic parameters (Table 1), the reshaping forces of the 4th to 7th stages are calculated respectively, and the reshaping force required to repair the deformed casing with the minimum diameter of 114 mm is 281.19 kN, as shown in Table 2.

3.1.3. Finite element calculation

Based on the structural dimensions of the reshaper and deformed casing, a parametric model is established. The casing is discretized into solid elements by the finite element method, and the target and contact elements are created on the outer surface of

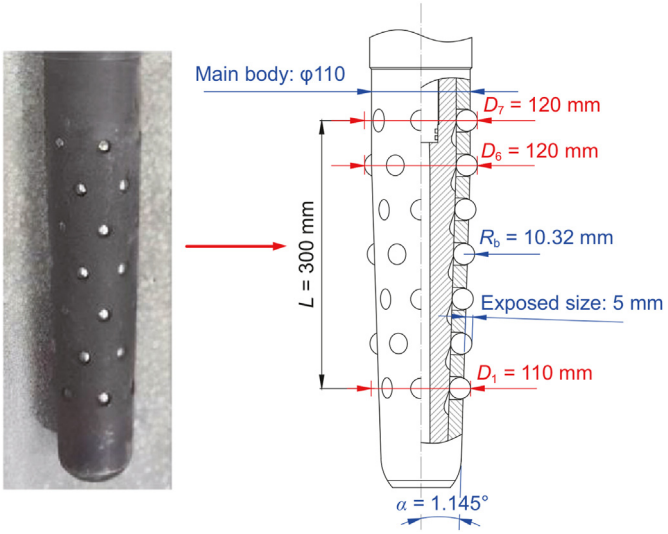

Fig. 10. Structural parameters of hydraulic rolling reshaper.

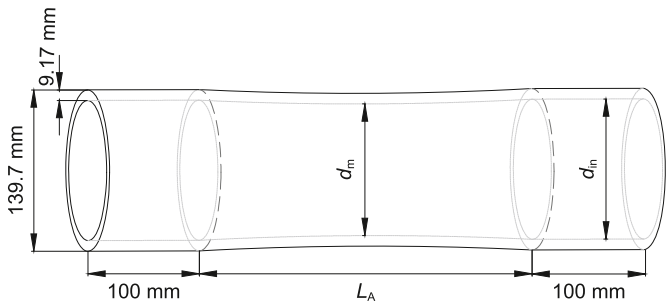

Fig. 11. Structural parameters of the deformed casing.

Table 1
Basic parameters of calculation.

Basic parameters, Units	L_A, mm	d_{in}, mm	n, /	k, /	L, mm	α, °	D_1, mm	v, mm·s^{-1}	ω, rad·s^{-1}
Value	300	121.36	7	4	300	1.145	110	1	0.48

Table 2
Calculated results of repairing force required for deformed casing (L_A = 300 mm, d_m = 114 mm).

Calculated parameters	D_i, mm	d_{mi}, mm	R_i, mm	t_i, s	S_i, mm^2	p_{bi}, MPa	F_i, kN
4th stage	116	114.0	3058.91	156.33	558.55	149.95	60.28
5th stage	118	115.5	3841.06	195.84	716.60	148.14	76.41
6th stage	120	117.5	5829.98	241.20	904.44	145.79	94.91
7th stage	120	119.5	12097.20	155.58	575.92	143.52	49.59
Total	–	–	–	–	–	–	281.19

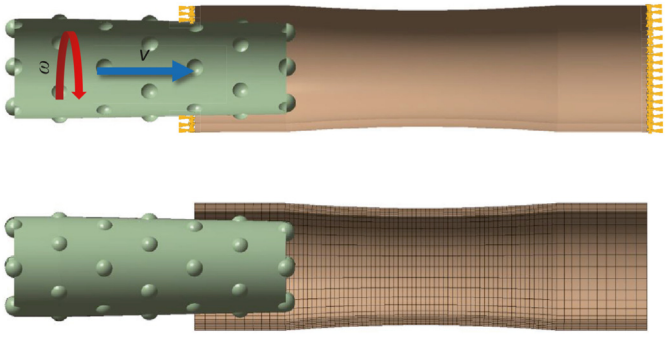

Fig. 12. Models of the repairing process. **(a)** Mechanical model. **(b)** Finite element model.

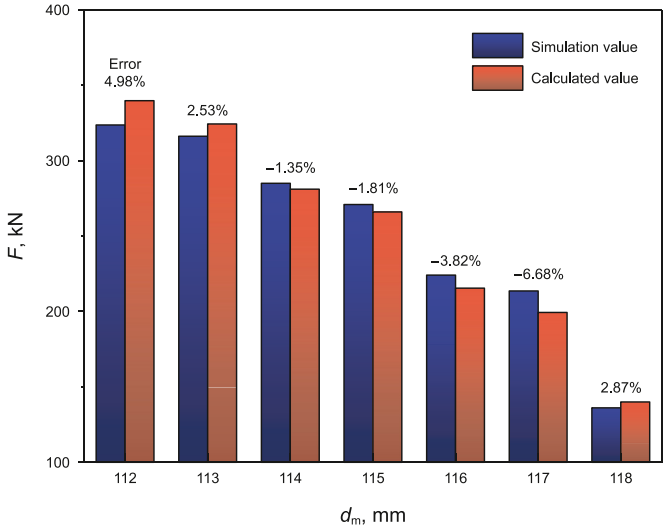

Fig. 13. Error (p_{bi}) of calculated and simulated results.

the reshaper and the inner surface of the casing, respectively. Furthermore, considering the computational cost and accuracy comprehensively, the global grid density is determined, and the key geometric features (such as the contact interface between the reshaper and the inner wall of the casing) are refined with the local grid refinement. According to the loading features of the integral structure, the end faces on both sides of the casing are set as fully fixed constraints, and the cylindrical joint is set up to simulate the motion relationship between the reshaper and the casing. In addition, to be consistent with the mathematical model, the initial position of the reshaper is set as follows: the cross-section where the first stage of the reshaper is located coincides with the cross-section of the connection between the deformed section and the intact section of the casing, and finally, the mechanical model and finite element model of hydraulic rolling reshaper repairing deformed casing are obtained, as shown in Fig. 12.

Since the elastic-plastic analysis is involved and the nonlinear characteristics of the contact area and pressure on the contact interface, the modified Newton-Raphson method is chosen to solve the nonlinear problems involved in the shaping process, which has been verified by our research group (Xu et al., 2020) through the combination of numerical simulation and experiment.

On this basis, the shaping process of the deformed casing with L_A = 300 mm and d_m = 114 mm is simulated, and the reshaping force required to repair the deformed casing is obtained to be 285.05 kN, which has a small error of −1.35% compared with the theoretical calculation.

3.2. Theoretical and numerical comparisons

To illustrate the reliability of Eq. (43), under the condition of a fixed axial deformation length (300 mm), p_{bi}^1, p_{bi}^2 and p_{bi} are used

Table 3
Comparison of calculated results with simulation data.

d_m, mm	Simulated results, kN	Theoretical results, kN			Error, %		
		p_{bi}^1	p_{bi}^2	p_{bi}	p_{bi}^1	p_{bi}^2	p_{bi}
112	323.65	364.17	315.38	339.78	12.52	−2.55	4.98
113	316.30	347.60	301.03	324.32	9.90	−4.83	2.53
114	285.05	301.38	261.00	281.19	5.73	−8.44	−1.35
115	271.00	285.19	246.98	266.08	5.23	−8.86	−1.81
116	224.08	230.99	200.05	215.52	3.09	−10.73	−3.82
117	213.60	213.64	185.02	199.33	0.02	−13.38	−6.68
118	136.15	150.12	130.00	140.06	10.26	−4.51	2.87

respectively to calculate the reshaping force required to repair the deformed casing with different minimum diameters, and the results of the corresponding finite element analysis are also listed as shown in Table 3. Remarkably, it can be seen that the error of the reshaping force calculated by using the average value (p_{bi}) is much smaller, which is all within 10% (Fig. 13), and the error is acceptable in engineering. Therefore, the above verification shows that the mathematical model established in this paper is reliable, which can effectively predict the magnitude of the reshaping force required to repair the deformed casing and provide a reference for on-site construction.

4. Analysis of the effects of parameters on the reshaping force

It can be observed from Eq. (43) that the reshaping force (F) is related to multiple parameters. According to the characteristics of the parameters, they are divided into three categories: the basic parameters of the deformed casing, the process parameters of the reshaper and the constructional dimensions of the reshaper. To investigate their influences on the reshaping force, the relationships between the reshaping force and each parameter are explored by the control variable method, and the influence degree of each parameter on the reshaping force is quantitatively analyzed by orthogonal simulation test combined with Pearson correlation coefficient.

4.1. Basic parameters of the deformed casing

The basic parameters of the deformed casing can be subdivided into the structural parameters of the deformed casing (L_A and d_m) and the material properties (σ_s and σ_b), and in the mathematical model developed in this paper, σ_s and σ_b of the casing with different materials are represented by the flow stress σ_f (Eq. (13)). Hence, for the three factors of L_A, d_m and σ_f, according to the control variable method, other variables are fixed, and only the influence of a single variable on the reshaping force is studied. To analyze their effects on the reshaping force clearly, the relationships between three variables and the reshaping force are plotted, as shown in Fig. 14.

At the same time, according to the central composite design method (Aksoy and Sagol, 2016; Chinthaginjala et al., 2022), the 3-factor 5-level orthogonal simulation test is designed on the premise of sufficient sample size, and the mathematical model established in this paper is used to calculate the reshaping force under the combination of various parameters.

On the basis of the calculation results, Pearson correlation coefficient is used to quantitatively reflect the degree of correlation between each parameter and the reshaping force (Ceballes and Abdelkefi, 2021; Zhong et al., 2018). The range of Pearson correlation coefficient is $[-1, 1]$, and the closer the correlation coefficient is to 1 or -1, the higher the degree of positive/negative correlation, which is calculated as follows:

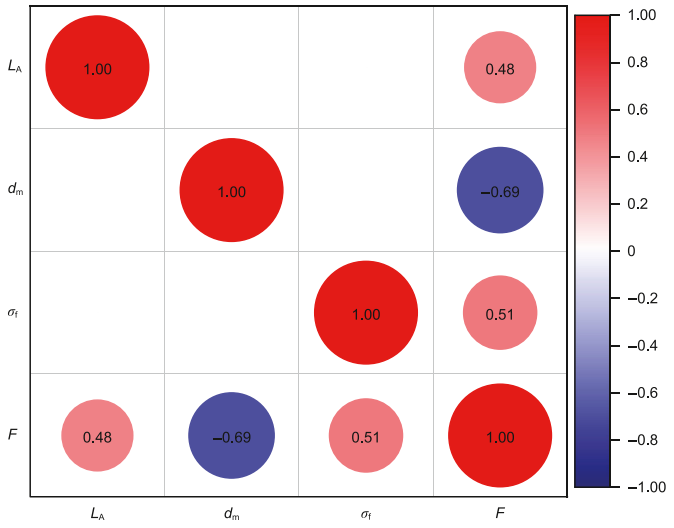

Fig. 15. Correlation heatmap of the basic parameters of the deformed casing and the reshaping force.

$$\rho(X,Y)=\frac{\mathrm{Cov}(X,Y)}{\sigma_X\sigma_Y}=\frac{\sum(X-\overline{X})(Y-\overline{Y})}{\sqrt{\sum(X-\overline{X})^2}\sqrt{\sum(Y-\overline{Y})^2}} \tag{44}$$

where ρ is Pearson correlation coefficient; $\mathrm{Cov}(X,Y)$ is the covariance; and σ_X and σ_Y are the standard deviations of variables X and Y, respectively.

According to the calculated results, the correlation heatmap is plotted as shown in Fig. 15. The scale on the right side indicates the color and depth of different correlation coefficients, and the color and diameter of different circles in the heatmap on the left side indicate the magnitude of correlation coefficients. It can be seen from Figs. 14 and 15 that the influence degree of the basic parameters of the deformed casing on the reshaping force from big to small is d_m, σ_f, L_A. Among them, both σ_f and L_A are positively correlated with the reshaping force, that is, the increase of σ_f and L_A will cause the increase of reshaping force. Moreover, d_m is negatively correlated with the reshaping force, that is, the smaller the minimum diameter of the deformed casing is, the greater the reshaping force is required. However, the basic parameters of the deformed casing are special in that they cannot be changed or improved during the shaping process.

4.2. Process parameters of the reshaper

According to the mathematical model, the process parameters of the reshaper include the axial translational velocity v, the rotating angular velocity ω, and the friction coefficient μ, and these

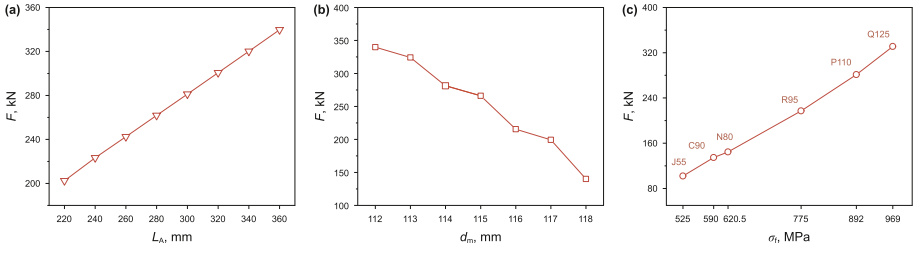

Fig. 14. Relationships between the basic parameters of the deformed casing and the reshaping force. **(a)** Axial deformation length of the deformed casing (L_A). **(b)** Minimum diameter of the deformed casing (d_m). **(c)** Flow stress (σ_f).

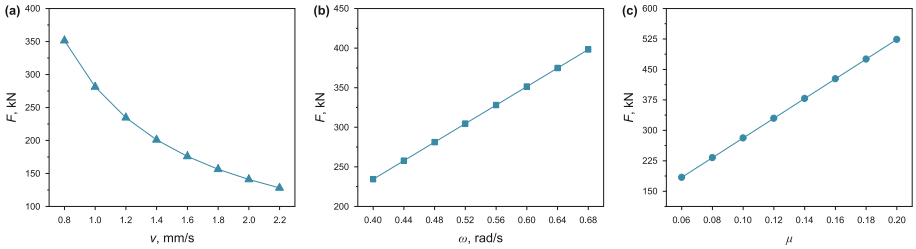

Fig. 16. Relationships between the process parameters of the reshaper and the reshaping force. **(a)** Axial translational velocity of the reshaper (v). **(b)** Rotating angular velocity of the reshaper (ω). **(c)** Friction coefficient (μ).

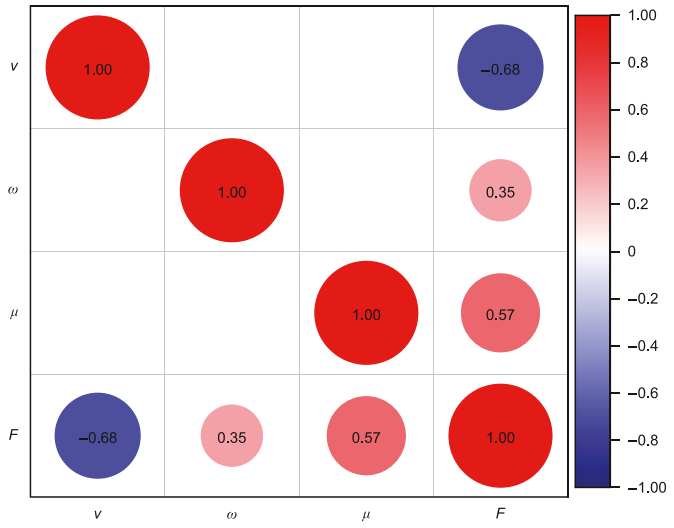

Fig. 17. Correlation heatmap of the process parameters of the reshaper and the reshaping force.

parameters can be adjusted in the shaping process. Similarly, the influence degree of each variable on the reshaping force is investigated respectively, and their relationships with the reshaping force are plotted in Fig. 16. In addition, the 3-factor 5-level orthogonal simulation test is also designed and calculated, and the correlation heatmap is plotted as shown in Fig. 17.

From Figs. 16 and 17, it can be seen that the influence degree of the process parameters of the reshaper on the reshaping force from big to small is v, μ, ω. Among them, both μ and ω are positively correlated with the reshaping force, that is, the reshaping force increases with the increase in μ and ω. Obviously, increasing the rotating angular velocity will significantly improve the uniformity of the casing, but the ground devices also need to provide greater reshaping force. Moreover, the friction coefficient has a greater impact on the reshaping force, but it is not advisable to reduce the friction coefficient blindly to reduce the reshaping force, because ensuring a certain friction can also transfer the reshaping force better and improve the efficiency of shaping. In addition, Figs. 16 and 17 show a negative correlation between v and the reshaping force, but excessive axial translational velocity will produce greater impact force, which will not only increase the risk of casing damage, but also make the deformation of the casing become uneven. Therefore, the axial translational velocity, the rotating angular velocity of the reshaper and the friction coefficient need to be reasonably matched with the structural dimensions of the reshaper and the actual condition, to ensure that the deformed casing can obtain better shaping effect.

4.3. Constructional dimensions of the reshaper

Based on the mathematical model, the constructional dimensions of the reshaper include the total length of the reshaper L, the total number of stages of the reshaper n, the number of balls per stage m, the taper of the reshaper α, the equivalent diameter of the first stage D_1, and the radius of the ball R_b. Therefore, considering the rationality of structure and combining with the relevant standard (ISO 3029−1:2014(E)), the relationships between individual variables and the reshaping force are investigated, and the curves of the reshaping force with each factor are obtained. The orthogonal test scheme of 3-factor 5-level is designed by orthogonal simulation test, and the correlation heatmap is drawn according to the calculated results, as shown in Figs. 18 and 19.

As can be seen from Figs. 18 and 19, the influence degree of the constructional dimensions of the reshaper on the reshaping force from big to small is D_1, n, α, m, L, R_b, and all of them are positively correlated with the reshaping force. Among them, D_1, n, α and m have a significant effect on the reshaping force. Therefore, in the structural optimization of hydraulic rolling reshaper, we should combine the actual application conditions of the reshaper, within the range of available reshaping force, and focus on the adjustment and optimization of these dimensions to further improve the shaping ability of the reshaper.

5. Conclusions

In this paper, the mechanical analysis on the process of repairing deformed casing by hydraulic rolling reshaper is carried out, which provides a new calculation method for solving the problem that the reshaping force often relies on empirical decision, and the influence of each calculated parameter on the reshaping force are analyzed in detail. Some interesting conclusions can be drawn from the results.

(1) Based on Hertz contact theory and elastic-plastic theory, a mathematical model for calculating the reshaping force required for repairing deformed casing by hydraulic rolling reshaper is established for the first time, which can be used to predict the reshaping force required to repair casing with any degree of deformation.
(2) Based on the structural characteristics and working principle of the hydraulic rolling reshaper, considering the contact nonlinear characteristics, the finite element model and numerical method for repairing deformed casing by hydraulic rolling reshaper are established, and the reliability and accuracy of the mathematical model are verified by several examples.
(3) According to the mathematical model, the relationships between multiple variables and reshaping force are discussed respectively, and the influence degree of each parameter on the reshaping force is analyzed and sorted by orthogonal

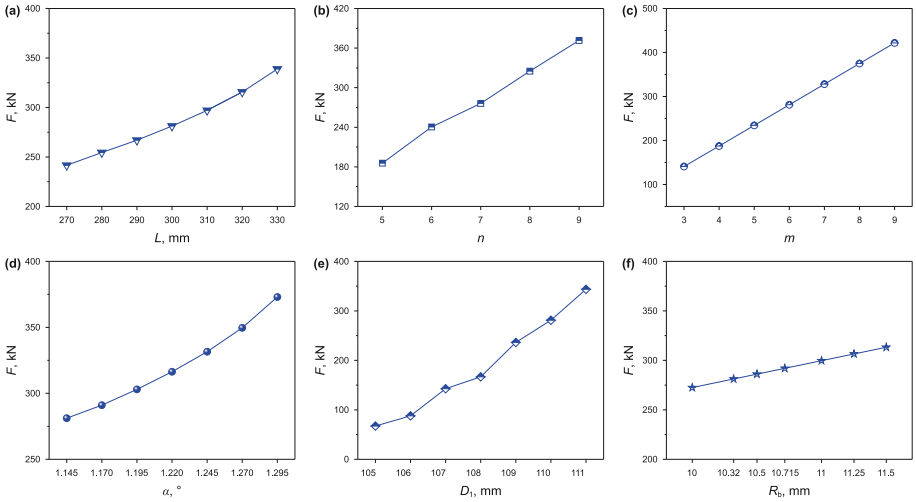

Fig. 18. Relationships between the constructional dimensions of the reshaper and the reshaping force. **(a)** Total length of the reshaper (L). **(b)** Total number of stages of the reshaper (n). **(c)** Number of balls per stage (m). **(d)** Taper of the reshaper (α). **(e)** Equivalent diameters of the first stage (D_1). **(f)** Radius of the ball (R_b).

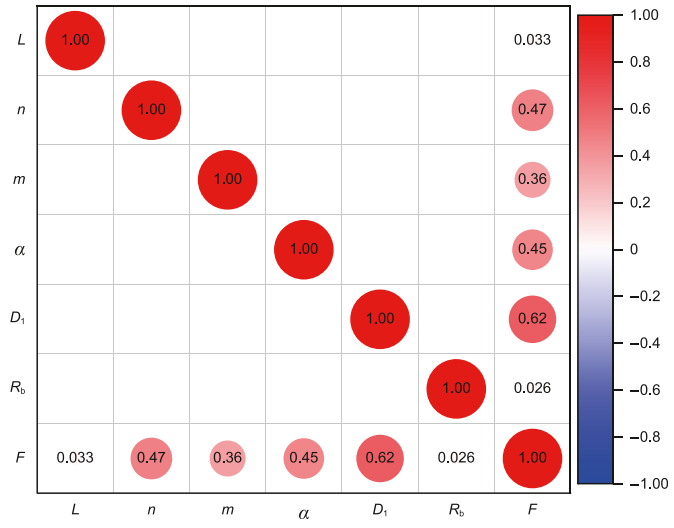

Fig. 19. Correlation heatmap of the constructional dimensions of the reshaper and the reshaping force.

simulation test and Pearson correlation analysis. Among them, for the basic parameters of the deformed casing: $d_m > \sigma_f > L_A$, for the process parameters of the reshaper: $\nu > \mu > \omega$, and for the constructional dimensions of the reshaper: $D_1 > n > \alpha > m > L > R_b$. In addition, L_A, σ_f, ω, μ and the constructional dimensions of the reshaper are positively correlated with the reshaping force, d_m and ν are negatively correlated with the reshaping force, and the research results provide a reference for the subsequent structural design and process optimization of the reshaper.

CRediT authorship contribution statement

Hong-Fei Li: Writing – review & editing, Writing – original draft, Validation, Methodology, Investigation, Formal analysis, Data curation, Conceptualization. **Min Luo:** Writing – review & editing, Supervision, Resources, Project administration, Methodology, Funding acquisition, Formal analysis, Conceptualization. **Ting-Ting Xu:** Writing – review & editing, Supervision, Investigation. **Qiao-Zhen Li:** Writing – review & editing, Supervision, Investigation. **Cong-Jian Huang:** Writing – review & editing, Data curation.

Declaration of competing interest

The authors declare that they have no known competing financial interests or personal relationships that could have appeared to influence the work reported in this paper.

Acknowledgment

This work was financially supported by the National Natural Science Foundation of China (51674088) and Natural Science Foundation of Heilongjiang Province of China (LH 2021E011).

References

Aksoy, D.O., Sagol, E., 2016. Application of central composite design method to coal flotation: modelling, optimization and verification. Fuel 183, 609–616. https://doi.org/10.1016/j.fuel.2016.06.111.

Ceballes, S., Abdelkefi, A., 2021. Application of sensitivity analysis and uncertainty quantification methods on the dynamic response of general nonlocal beams. Appl. Math. Model. 97 (9), 322–343. https://doi.org/10.1016/j.apm.2021.03.057.

Chinthaginjala, H., Telkar, M.B., Hindustan, A.A., et al., 2022. Formulation development and optimization of famotidine mucoadhesive tablets by central composite design. Indian J. Pharm. Educ. 56 (4), 1044–1051. https://doi.org/10.5530/ijper.56.4.185.

Denney, D., 2012. Expansion-cone material: heat-treatment effects. J. Petrol. Technol. 64 (6), 110–114. https://doi.org/10.2118/0612-0110-jpt.

Deng, K.H., Lin, Y.H., Zeng, D.Z., et al., 2016. Theoretical study on working mechanics of Smith expansion cone. Arabian J. Sci. Eng. 41 (11), 4283–4289. https://doi.org/10.1007/s13369-016-2097-3.

Deng, K.H., Liu, W.Y., Lin, Y.H., et al., 2018. Experimental and numerical investigation on repairing process of cement-casing repaired by rolling reshaper. J. Petrol. Sci. Eng. 166, 305–312. https://doi.org/10.1016/j.petrol.2017.11.056.

Deng, K.H., Liu, W.Y., Liu, B., et al., 2019. Repairing force for deformed casing shaping with spinning casing swage and damage behaviour of cement sheath. Appl. Math. Model. 70 (6), 425–438. https://doi.org/10.1016/j.apm.2019.01.042.

Forbes, M., 2021. Optimizing production and improving well accessibility with expandable technology. J. Petrol. Technol. 73 (7), 37–38. https://doi.org/10.2118/0721-0037-jpt.

Harris, T.A., Kotzalas, M.N., 2007. Rolling Bearing Analysis: Essential Concepts of Bearing Technology, fifth ed. Taylor & Francis Group, New York, US.

Han, G., Tan, Z., An, Y., 2018. Workover Engineering, second ed. Petroleum Industry Press, Beijing, China. (**in Chinese**).

Jiang, M.Z., 2003. Study the Repairing Force and Damage Mechanism for the Cement Loop during Repairing Destroyed Casing. Ph.D. Thesis. Harbin Engineering University, Harbin, China, pp. 1–10 (in Chinese).

Jin, C.J., 2022. Mechanical Analysis and Structural Optimization of the Shaping

Necking Sleeve of the Hydraulic Ball Shaper. M.Eng. Thesis. Northeast Petroleum University, Daqing, China, pp. 24–29. https://doi.org/10.26995/d.cnki.gdqsc.2022.000467 (in Chinese).
Liu, C.S., Sun, C., Wang, Q.P., et al., 2011. The development and application of the hydraulic casing ball shaper. China Pet. Mach. 39 (11), 55–56. https://doi.org/10.16082/j.cnki.issn.1001-4578.2011.11.022 (in Chinese).
Lin, Y.H., Deng, K.H., Zeng, D.Z., et al., 2013. Numerical and experimental study on working mechanics of pear-shaped casing swage. Adv. Mech. Eng. 5, 893723. https://doi.org/10.1155/2013/893723.
Li, T.L., 2014. Applied Elastoplastic Mechanics. China University of Geosciences Press, Wuhan, China (in Chinese).
Lin, M.Q., 2016. Design and Research on Hydraulic Spring Combined Deformed Casing Repair Device. M.Eng. Thesis. China University of Petroleum (East China), Qingdao, China, pp. 425–438 (in Chinese).
Luo, M., Zhao, T.T., Gu, H.W., et al., 2016. Study on radial repair force of reducing deformation casing. Mach. Des. Manuf. Eng. 45 (5), 77–80. https://doi.org/10.3969/j.issn.2095-509X.2016.05.017 (in Chinese).
Lei, Q., Li, Y.L., Li, T., et al., 2020. Technical status and development direction of workover operation of PetroChina. Petrol. Explor. Dev. 47 (1), 161–170, 10.1016S1876-3804(20)60015-5.
Peng, S.P., Fu, J.T., Zhang, J.C., 2007. Borehole casing failure analysis in unconsolidated formations: a case study. J. Pet. Sci. Eng. 59 (3), 226–238. https://doi.org/10.1016/j.petrol.2007.04.010.
Tao, L., 2015. Solid expandable tubular patching technique for high-temperature and high-pressure casing damaged wells. Petrol. Explor. Dev. 42 (3), 408–413. https://doi.org/10.1016/S1876-3804(15)30032-X.
Wu, Q., Liu, H., 2005. Optimum design of impact construction technology for casing damaged wells. China Pet. Mach. 33 (2), 11–14. https://doi.org/10.3969/j.issn.1001-4578.2005.02.004 (in Chinese).
Wang, R., Huang, W.B., Huang, Z.P., 2006. Introduction to Elasticity and Plasticity. Peking University Press, Beijing, China (in Chinese).
Wang, K.Y., Deng, J.G., Yan, W., et al., 2022. Study on geometric characteristics and quantitative description method of casing deformation during shale reservoir hydraulic fracturing. Energies 15 (6), 2280. https://doi.org/10.3390/en15062280.
Xu, Z.L., 2006. Elasticity Mechanics, fourth ed. Higher Education Press, Beijing, China (in Chinese).
Xu, B.G., Zhang, Y.P., Wang, H., et al., 2009. Application of numerical simulation in solid expandable tubular repair for casing damage wells. Petrol. Explor. Dev. 36 (5), 651–657. https://doi.org/10.1016/s1876-3804(09)60152-x.
Xu, T.T., Luo, M., Chi, X., et al., 2020. Mechanical analysis and single shaping limit research of casing rolling shaping. Mach. Tool. Hydrau. 48 (5), 88–92. https://doi.org/10.3969/j.issn.1001-3881.2020.05.019 (in Chinese).
Yu, H.S., Wang, C.B., Yang, G.S., et al., 2011. Study situation of expandable casing technology and the working principle. Drill Eng 38 (3), 1–4. https://doi.org/10.3969/j.issn.1672-7428.2011.03.001 (in Chinese).
Yu, H.M., 2017. Application of grading anti-sticking hydraulic casing shaping technology in workover operation. Chem. Eng. Manag. 20 (7), 220. https://doi.org/10.3969/j.issn.1008-4800.2017.20.203 (in Chinese).
Zhu, X.K., Leis, B.N., 2005. Influence of yield-to-tensile strength ratio on failure assessment of corroded pipelines. J. Press. Vess-T. ASME. 127 (4), 436–442. https://doi.org/10.1115/1.2042481.
Zhang, P.H., 2011. Force Analysis of Electromagnetic Shaping Process of Petroleum Casing. M.Eng. Thesis. Northwest University, Xi'an, China, pp. 19–26 (in Chinese).
Zhong, J.Q., Liu, L.Y., Sun, Q., et al., 2018. Prediction of photovoltaic power generation based on general regression and back propagation neural network. Energy Proc. 152 (10), 1224–1229. https://doi.org/10.1016/j.egypro.2018.09.173.
Zhou, F.C., Wang, T., Ma, C.Q., et al., 2019. Review on the evaluation of casing damage level in oil and gas field. MATEC Web Conf 256, 02008. https://doi.org/10.1051/matecconf/201925602008.